Received: August 9, 2023. Revised: September 27, 2023.

International Journal of
Intelligent Engineering & Systems

http://www.inass.org/

Crowbar With a Parallel R_pL_p Configuration Using PI Controller to Solve the Problem of DFIG-Wind Farm Stability During a Symmetrical Fault

Azeddine Loulijat[1]* **Mouncef El Marghichi[1]** **Mohamed Makhad[2]** **Naoufl Ettalabi[1]**

[1]*Hassan I University, Settat, Morocco*
[2]*Mohammed V University, Rabat, Morocco*
* Corresponding author's Email: rehalloulijat@gmail.com

Abstract: The doubly fed induction generator (DFIG) is particularly sensitive to grid faults, representing a significant drawback of this generator type, because of the direct connection of its stator windings to the network. The electromagnetic coupling between the stator and rotor in the DFIG results in an undesirable consequence, where voltage dips lead to excessive stator current, causing high currents in sensitive inverters and overloading the DC-link condenser. This document outlines a comparative study that examines two protection scheme configurations with a proportional-integral (PI) controller for managing transient rotor current and overcharging of the DC-link capacitor in order to optimize the operation of the DFIG during network faults. One conventional design choice combines a crowbar circuit with a DC-chopper, in contrast the other design option proposes integrating a modified protection scheme (MPS) that includes an R_pL_p parallel circuit with the traditional crowbar. Both schemes are placed between the rotor windings and the rotor-side converter (RSC) to boost the low voltage ride-through (LVRT) capacity of the generator. The comparison of results obtained through MATLAB/SIMULINK simulations reveals the successful performance of these two schemes in reducing elevated intensity current of rotor and DC-link voltage levels in the DFIG machine. Furthermore, the traditional crowbar and MPS circuit design have effectively limited the current intensity of the RSC converter to levels lower than 0.22 kA and 2.95 kA, while absorbing up to 2.53 kA and 1.53 kA respectively. Thus, ensuring that the DC-link tension stays within the safe range when network failures occur. The notable distinction is that the MPS design prevents the decoupling of the rotor from the RSC during a symmetrical voltage dip, enabling effective control of all stator power through the RSC.

Keywords: Wind farm, Doubly fed induction generator, Symmetrical voltage dip, Low voltage ride-through, Proportional-integral control, Conventional crowbar, DC-chopper, Modified protection scheme, R_pL_p parallel circuit.

1. Introduction

Due to the escalating consumption of electricity from fossil fuels and nuclear power, which poses environmental risks, scientists are driven to seek sustainable solutions. Wind energy has emerged as a significant and challenging source of green energy in the global economy [1, 2]. One of the various categories of wind power generation systems, DFIG is presently the preferred widely utilized technology, especially in wind energy production units with capacities exceeding 1MW, as illustrated in Fig. 2 [3, 4]. On the other hand, the DFIG is an asynchronous generator with a coils rotor where its stator is attached to the electrical network without the need for a power supply, and the rotor is attached to the electrical network through two inverters (reversible static power frequency converters) [5]. By employing a control system to manage the converters, it becomes possible to constantly enhance power output by identifying the optimal point where maximum power generation occurs (maximum power point tracking (MPPT) strategy) [6].

The DFIG's reliance on power electronics and its connection to the power network makes it susceptible to network faults, especially during episodes of voltage dips in the grid. As a result, this can lead to elevated peaks in current in the stator, fluctuations in both the active and reactive power of the stator, and variations in the electromagnetic torque[7, 8]. In

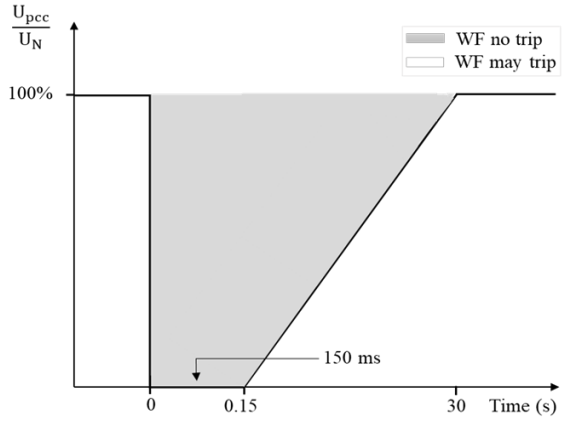

Figure. 1 The specifications for LVRT at the PCC

addition, the robust electromagnetic linkage enter the stator and rotor enables efficient transmission of peak currents from the rotor to the sensitive power inverters. If this situation arises, it could result in the DC-link condenser being overcharged and the rotor converters operating beyond their safety limits. As a result, the converters may undergo degradation, and the user may not have access to the DFIG's power control capabilities even after the fault has been resolved. The initial concept to prevent damage to the converter caused by a symmetrical fault was to disconnect the DFIG from the network. The high degree of incorporation of wind turbines into the electric system presents challenges in restoring network voltage due to their significant presence. This leads that network experts developing strict network codes that demand that wind turbines remain connected in case of a network fault and, in some instances, provide reactive energy to the electrical grid to help restore its level of tension [9]. Fig.1 presents the LVRT curve described in this document, which dictates that wind turbines must maintain network connection during short-circuit faults, as long as the tension at the point of common coupling (PCC) remains above the continuous voltage line [10].

To guarantee continuous network connectivity amidst disruptions, it's imperative for the system to incorporate fault ride-through (FRT) techniques that provide it with the capability to surmount faults. A plethora of distinct FRT methodologies have been suggested in existing literature and can be categorized as follows: the inclusion of supplementary protective mechanisms, such as the crowbar technique [11-13], crowbar with series dynamic braking resistors (SDBR) [14, 15], and crowbar with DC-chopper [3, 7, 10, 16-20]; as well as the deployment of reactive power supply solutions like the static synchronous compensator (STATCOM) [21, 22] and dynamic voltage restorer (DVR) [23].

For the present work, a MPS of the DFIGs system is suggested to improve its LVRT capability and then compared with the crowbar accompanied by a DC-chopper in the course of voltage dip. The MPS incorporates one crowbar assembly with a parallel of R_pL_p devices with not using a DC-chopper circuit for limited DC-link tension as in the [3, 7, 10, 16-20], collected from the rotor coils to the RSC under symmetrical voltage dip conditions. In addition, we avoided using the DC-chopper circuit with a better choice of R_pL_p values in several simulation results. Finally, the reduction of the high rotor current, the limited intermediate circuit voltage, and the sustainment of the RSC connection to the rotor are successfully achieved. Furthermore, the generator is partially made as DFIG, so it has minimized the demand of reactive energy to the network and keeps the regulation of the reactive and active stator output power, compared to the classic scheme based on a crowbar with a DC-chopper, this is advantageous.

The document consists of multiple sections, the bibliography is discussed in section 2. Namely, section 3 covers the modeling and control with PI controller of wind turbine and DFIG, followed by section 4 where we propose an against excessive rotor current protection scheme for DFIG and demonstrate its effectiveness by comparing it with the traditional method in a MATLAB/Simulink-based simulation of a symmetrical voltage dip in section 5. Lastly, section 6 presents the conclusion of the document.

2. Examination of relevant literature

Table 1 lists research into the drawbacks of techniques used to protect a DFIG-based wind farm (WF) against voltage dips. The predominant protective device employed is the "crowbar with DC-chopper" type resistor. This crowbar linked in series through an insulated-gate bipolar transistor (IGBT) switch with the rotor windings. Additionally, the DC-chopper includes a unique resistor connected in parallel via an IGBT switch to the DC-link capacitor. During faults, the RSC becomes decoupled from the rotor, leading the collector rings to shift towards the crowbar resistors. Consequently, the DFIG's behavior resembles that of a generator with a squirrel cage, necessitating reactive energy from the network, which induces a voltage drop at the connection point in the park. Furthermore, the disconnection of the RSC from the rotor leads to the loss of active and reactive stator power regulation.

To tackle the difficulties identified in literature regarding the use of the "crowbar with DC-chopper technique", it is proposed to employ an MPS technique. This technique enhances the DFIG's

Table 1. Drawbacks of the techniques utilised

Technique applied	Drawbacks
Crowbar [11-13]	❖ Crowbar activation leads to a loss of control over the RSC.
Crowbar with DC-chopper [3, 7, 10, 16-20]	❖ Crowbar activation leads to a loss of stator power control over the RSC. ❖ Behavior of a DFIG is similar to that of a generator with a squirrel cage, requiring reactive energy from the grid, which results in a voltage drop at the park's connection point. ❖ Duration required for converter disengagement and subsequent restoration exceeded that of a crowbar activation.
Crowbar with SDBR [14, 15]	❖ Adequacy of voltage quality might vary based on the selected SDBR switching scheme.
STATCOM[21, 22]	❖ Increased capital outlay and ongoing operational expenses. ❖ Applying the present restriction using injection.
DVR[23]	❖ During a fault, the DVR requires the surplus active power produced by the wind generator to be assimilated, achieving the desired level of V_{dc}. ❖ Demands enough energy storage capacity to address voltage sags effectively.

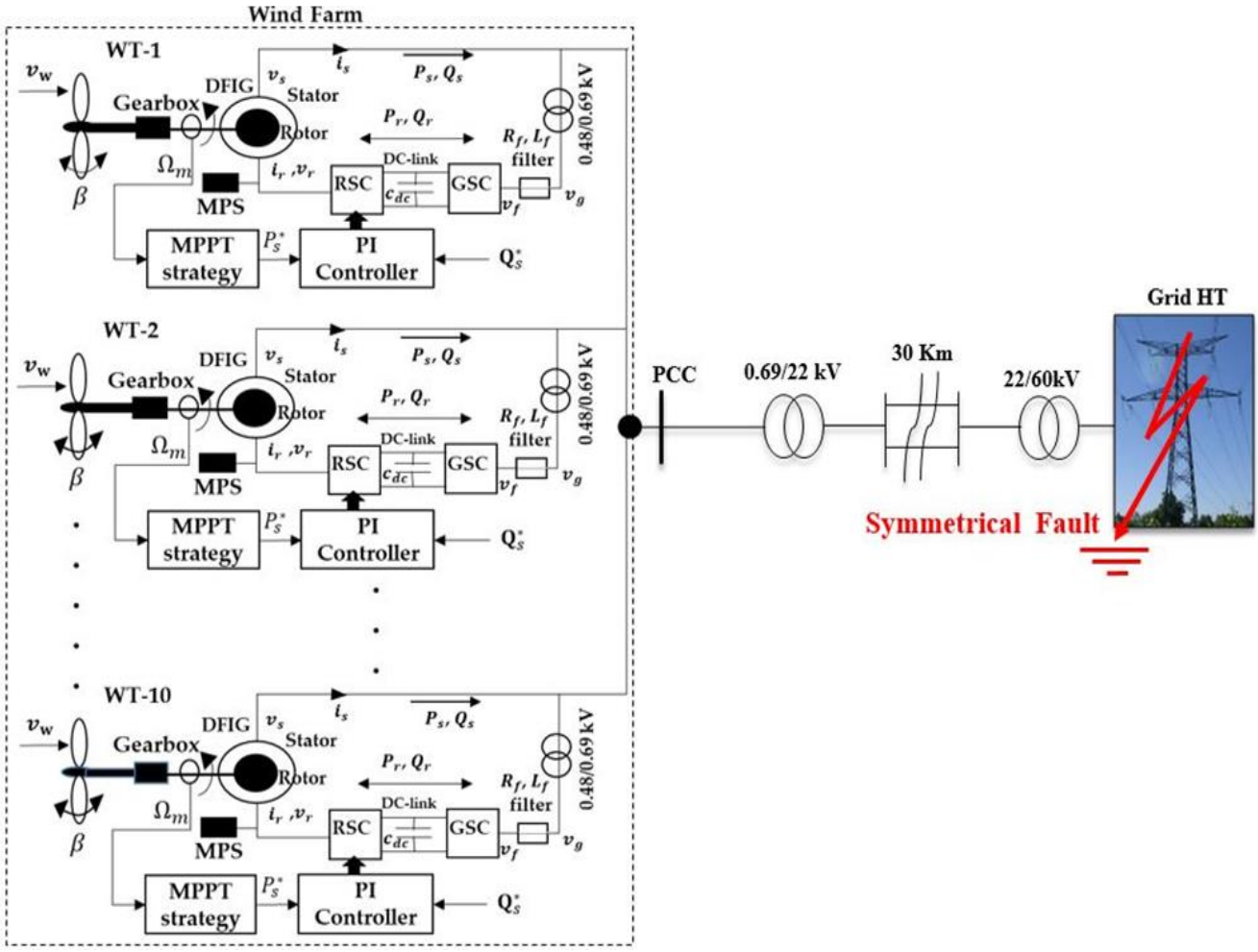

Figure. 2 DFIG-wind farm configuration

behavior, while also maintaining the connection between the rotor and RSC. This facilitates control over the active and reactive power being injected into the grid.

3. Wind farm system modelling

The WF described contains 10 wind turbines that utilize windings in the rotor of induction generators in conjunction with a 3-phase power system. The stator coils of these generators are linked directly to the grid. To connect the rotor coils to the electrical networks, a variable frequency alternating current(AC)/ direct current (DC)/AC power inverter is employed, which includes the RSC, DC-link, grid-side converter (GSC) , and $R_f L_f$ filter components as

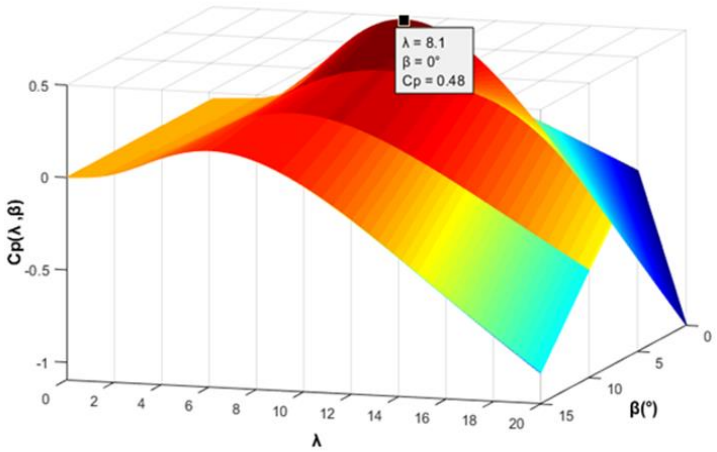

Figure. 3 3D plot of C_p

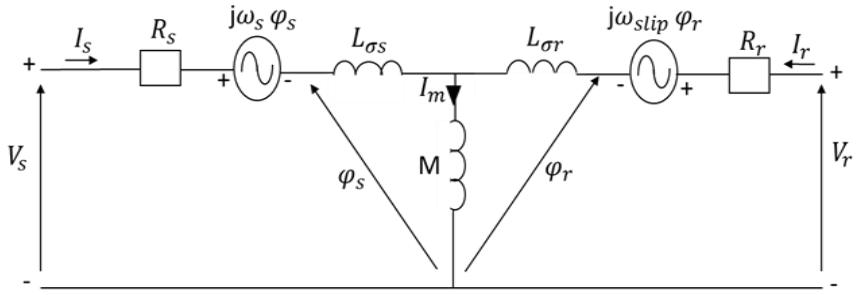

Figure. 4 Circuit model for the back-to-back converter

depicted in Fig. 2.

3.1 Turbine model and MPPT strategy

The wind turbine model generates the captured mechanical power (P_{cap}), written by this equation:

$$P_{cap} = \frac{1}{2} C_p(\lambda, \beta) \rho S_t v_w^3 \quad (1)$$

Considering S_t as the area swept by the turbine and ρ as the air mass density, respectively. The angle of the stall and the speed ratio are β and λ respectively. The power coefficient (C_p) and wind speed (v_w) are represented accordingly.

In this research article, the power coefficient model is defined as in [24]:

$$C_p(\lambda, \beta) = 0.5176 \left(\frac{116}{\lambda_i} - 0.4\beta - 0.5\right) . e^{\left(\frac{-21}{\lambda_i}\right)} + 0.0068\lambda \quad (2)$$

With:

$$\begin{cases} \frac{1}{\lambda_i} = \frac{1}{\lambda + 0.08\beta} - \frac{0.035}{\beta^3 + 1} \\ \lambda = \frac{R\omega_r}{v_w} \end{cases} \quad (3)$$

With the DFIG, we can capture the maximum wind power at the optimum tip speed (λ_{opt}), as demonstrated in Eq. (4). In addition, the MPPT curve is used in the mechanical speed of generator controller as in [24], which is determined by replacing Eqs. (3) to (1).

$$P_{MPPT} = P_s^* = \frac{1}{2} C_{p,max} \rho S_t \left(\frac{R\omega_r}{\lambda_{opt}}\right) \quad (4)$$

By keeping λ and β at their optimal values, the maximum C_p value is attained. It is observed in the Fig. 3 above that $C_p(\lambda,\beta)$ = 0.48 for λ_{opt} = 8.1 and β_{opt} = 0.

3.2 Model of DFIG and RSC converter

Eqs. (5) to (8), as documented below [7, 10], can be used to document both the voltages and fluxes of the stator by utilizing both the DFIG-circuit model (depicted in Fig. 4) and the reference synchronous frame, which is set to remain stationary at the stator flux level.

$$V_s = R_s I_s + L_s \frac{dI_s}{dt} + M \frac{dI_r}{dt} + j\omega_s \varphi_s \quad (5)$$

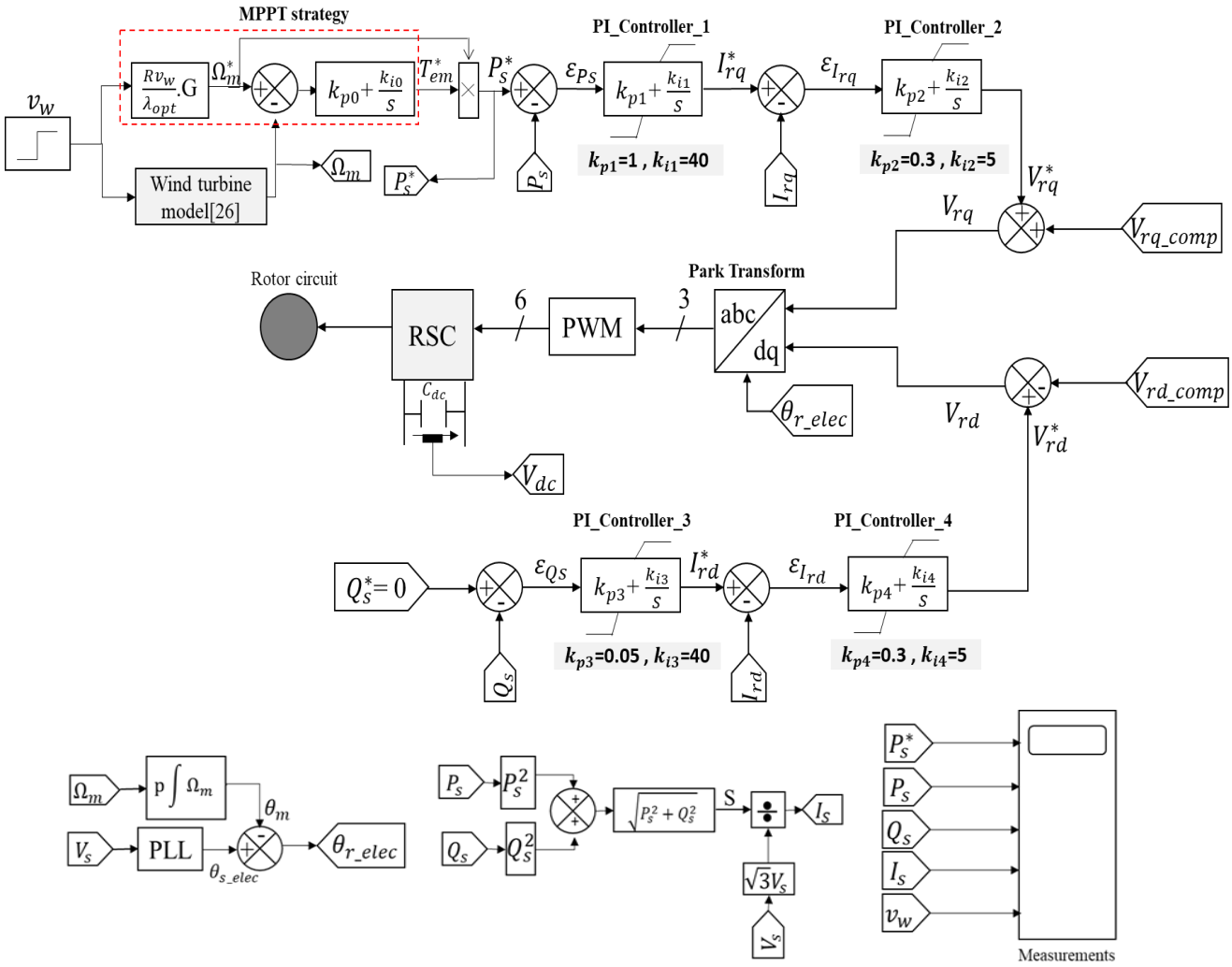

Figure. 5 Scheme of the RSC controller

$$V_r = R_r I_r + L_r \frac{dI_r}{dt} + M \frac{dI_s}{dt} + j\omega_{slip}\varphi_r \quad (6)$$

$$\varphi_s = L_s I_s + M I_r \quad (7)$$

$$\varphi_r = L_r I_r + M I_s \quad (8)$$

See Fig. 2, both the tension and power of the converter, P_S and Q_S in the direct-quadrature(dq) framework, which is set at the stator flux and the AC voltage of the network, respectively, are written in Eqs. (9) and (10) [7]:

$$P_s = \frac{3}{2}\left(V_{sd} I_{sd} + V_{sq} I_{sq}\right) \quad (9)$$

$$Q_s = \frac{3}{2}\left(V_{sq} I_{sd} - V_{sd} I_{sq}\right) \quad (10)$$

3.3 Design of DFIG-RSC controller

The RSC may deliver a variable steady-state frequency to the DFIG rotor and thus vary its speed of rotation. In addition, the RSC commands the supply of active and reactive outputs energy to the stator using the rotor's dq current values. So the above equations become the following:

$$P_s = \frac{3}{2} V_s \frac{M}{L_s} I_{rq} \quad (11)$$

$$Q_s = \frac{3}{2} V_s \frac{M}{L_s} I_{rd} - \frac{V_s^2}{L_s \omega_s} \quad (12)$$

Eqs. (11) and (12) above can be derived to express the relation between the current of rotor dq components and the stator power outputs P_s and Q_s in the reference system aligned with the static flux. For this application, RSC is used to ensure both velocity control (output power from the stator) and to monitor reactive energy(terminal voltage) as depicted in Fig. 5. For decoupling active and reactive power output from the stator by rotor current command, the 3-phase instantaneous i_{r_abc} are taken and then converted to I_{rd} and I_{rq} using a reference stator flux-oriented framework. To achieve this, the references

for I_{rq} and I_{rd} (noted I^*_{rq} and I^*_{rd}) are determined using the power controllers for both active and reactive output values, respectively. To generate the real error values, the real currents I_{rd} and I_{rq} are measured in comparison to their corresponding reference values, The measured error values are subsequently fed into the PI regulators, which in turn generate the command signals V_{rq} and V_{rd}. The associated cross-coupling terms V_{rd_comp} and V_{rq_comp} are used to correct the two command voltage signals, resulting in the output magnitudes V_{rd} and V_{rq}. This output is processed by the pulse width modulation (PWM) unit to deliver gate commands for IGBT to drive the RSC.

3.4 DFIG behavior under voltage dip situation

A sudden drop in stator tension to a lower level causes a surge in rotor current and intermediate circuit DC-link tension. These surges, while lasting just a brief time, can destroy both the RSC and the linking DC-condenser. This is primarily due to the low capacity of the converter, which is not able to generate the necessary voltage to command the generator. Also, in Eq. (13) [25], the relation of both stator and rotor tension is shown:

$$V_s = M\left(1-\frac{L_s L_r}{M^2}\right)\frac{dI_r}{dt} + j\left(\omega_s \varphi_s - \frac{L_s}{M}\omega_{slip}\varphi_r\right) + \frac{L_s}{L_r}V_r \quad (13)$$

Under steady-state conditions, $\frac{dI_r}{dt} = 0$, and Eq. (13) goes to Eq. (14).

$$V_s - j\left(\omega_s \varphi_s - \frac{L_s}{M}\omega_{slip}\varphi_r\right) = \frac{L_s}{L_r}V_r \quad (14)$$

When the fault appears, an abrupt change in the AC voltage ΔV_s is observed. However, in the moment of appearance of the default, the stator and rotor fluxes will not vary abruptly because $\varphi_s = \int V_s\ dt$ and $\varphi_r = \int V_r\ dt$. Regarding Eq. (13), the change in this second mandate will not be abrupt, and, consequently, at the moment when a failure appears, the variation of the stator tension may be written in the following manner:

$$\Delta V_s = M\left(1-\frac{L_s L_r}{M^2}\right)\frac{dI_r}{dt} + \frac{L_s}{L_r}\Delta V_r \quad (15)$$

To maintain $\frac{dI_r}{dt} = 0$ during the default, there needs to be a great change in step in the rotor voltage ΔV_r to keep up with the change in the stator voltage. Nevertheless, the RSC is unable to generate the requested ΔV_r because the RSC's maximum voltage capacity is only around 30%. As a result, a significant overcurrent will be caused in the winding of the rotor,which requires protection.

4. Safeguarding against excessive rotor current

The following section outlines the modified protection scheme suggested for rotor current in DFIG. The most usually used DFIG security device is a crowbar (with DC-chopper) which is deployed to operate in a timing sequence (Fig. 6(a)). It is one of many preferred strategies for the reduction of surge currents in the rotor due to its high reliability, reduced cost, and easy integration. However, enabling the crowbar ($IGBT_{crw}$ ON) in case of a grid failure stops the RSC ($IGBT^{c}_{rsc}$OFF) from functioning, causing a complete disruption of generator control. In this situation, the generator is similar to a squirrel cage induction generator (SCIG) with high-resistance working with a very strong slip, which leads to a high demand for reactive energy. This elevated level of reactive energy request removes the voltage at the PCC.

4.1 Modified protection scheme (MPS)

A schematic diagram of a suggested rotor protection scheme used to boost the LVRT of the DFIG for the time of electric system perturbations is shown in Fig. 7(a). This consists of the combination of a crowbar and a device from the R_pL_p parallel circuit. In the event that the rotor current exceeds its maximum limit, the modified diagram is implemented on the rotor windings at position M ($IGBT_{MPS1}$ ON), and the RSC terminal is relocated to position N($IGBT_{MPS2}$ ON). At this juncture, the upper rotor current (I_r^f) is distributed between the crowbar current (I_{crw}^{MPS}) and the current flowing through the RSC (I_{rsc}^{MPS}). The magnitude of the current of crowbar is depended by the size of the crowbar resistor (R_{crw}^{MPS}), while the current through the RSC is influenced by the impedance of the R_pL_p device ($Z_{parallel}$). By not considering the switching maneuvers during the trip and elimination of faults, the RSC remains connected to the rotor coils for the duration of the DFIG's operation. Moreover, upon activation of the MPS, the rotor windings of the generator are divided, with a portion being bypassed through the crowbar and another portion being connected to the RSC. An automatic command with PI controller of the generator output through the RSC is kept, which is a benefit compared to the traditional crowbar (with DC-chopper). Furthermore, this type of protection with rotor coils partially shorted through the crowbar

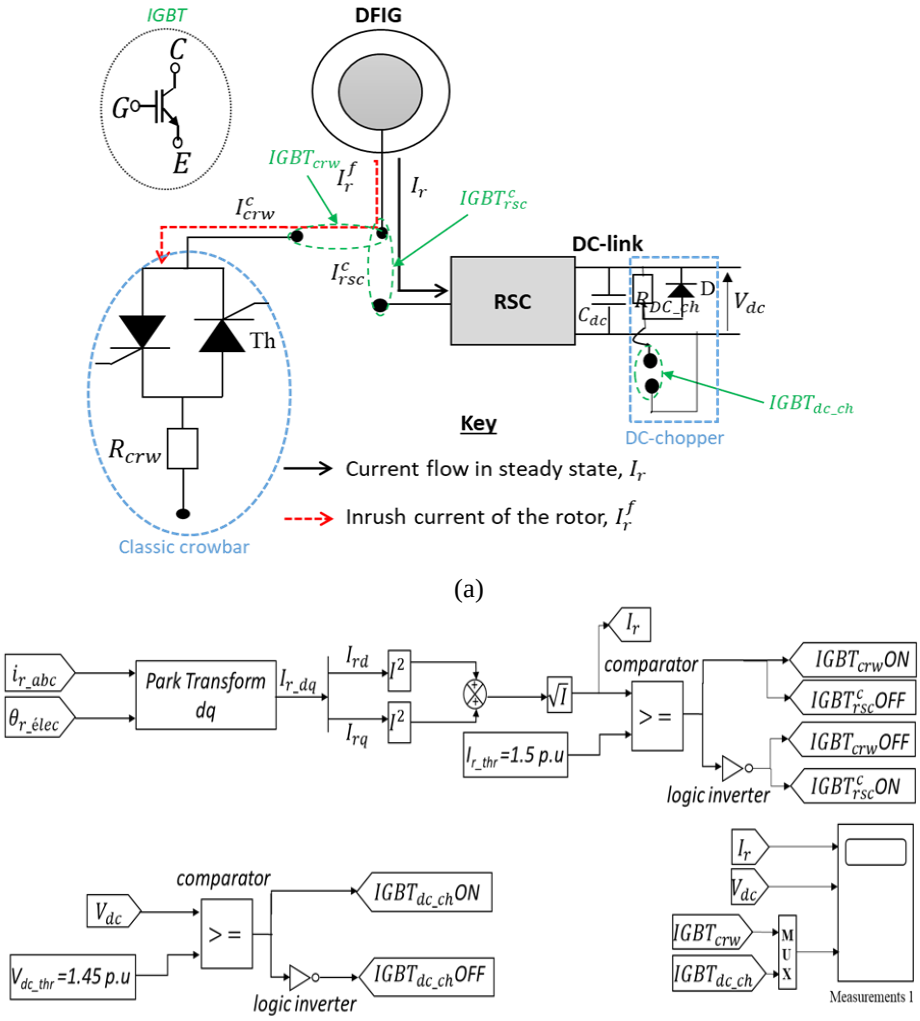

Figure. 6 Commutation architectures for: (a) traditional crowbar with DC-chopper scheme and (b) their IGBT's command algorithms

and partially collected to the RSC converter through the R_pL_p is making a temporal mode of the generator. During this phase, the machine exhibits characteristics of both a wound rotor induction generator and a SCIG, as the MPS is in operation. The MPS can become a typical crowbar if a big parallel impedance is selected with $R_{crw}^{MPS} = R_{crw}$ (resistance of crowbar traditional) used. However, this is contingent on the R_pL_p parameters and the resistance of crowbar (R_{crw}^{MPS}). On the contrary, if a low $Z_{parallel}$ is used and a high crowbar resistance is chosen, the overcurrent of the rotor circulates in the R_pL_p circuit to the converter that might be destroyed. So, it is required to preserve the ideal settings of both R_{crw}^{MPS} and R_pL_p to achieve the MPS goals.

5. Simulation results

The technique that we suggested is explored in this subsection using compilation studies with a MATLAB/Simulink environment. One wind turbine of DFIG with both RSC and GSC physically spaced through the DC-link is emulated as a single two-mass unit where the parameter settings of the DFIG are found in[10] (Table 3 in appendix).

5.1 Results on extracted power

A wind profile as a step was considered to achieve this, as depicted in Fig. 8. The results of the simulation are displayed in the next sections. Initial wind speed of 5.1 m/s increases to 11m/s after 3.4 seconds. In Fig. 9, the power extracted using the MPPT strategy (stator power reference) varies as a function of wind speed.

5.2 Results of the comparison under the condition of a balanced voltage dip fault

At t=7.5s, a symmetrical voltage dip fault occurred over a distance of more than 30 km from the

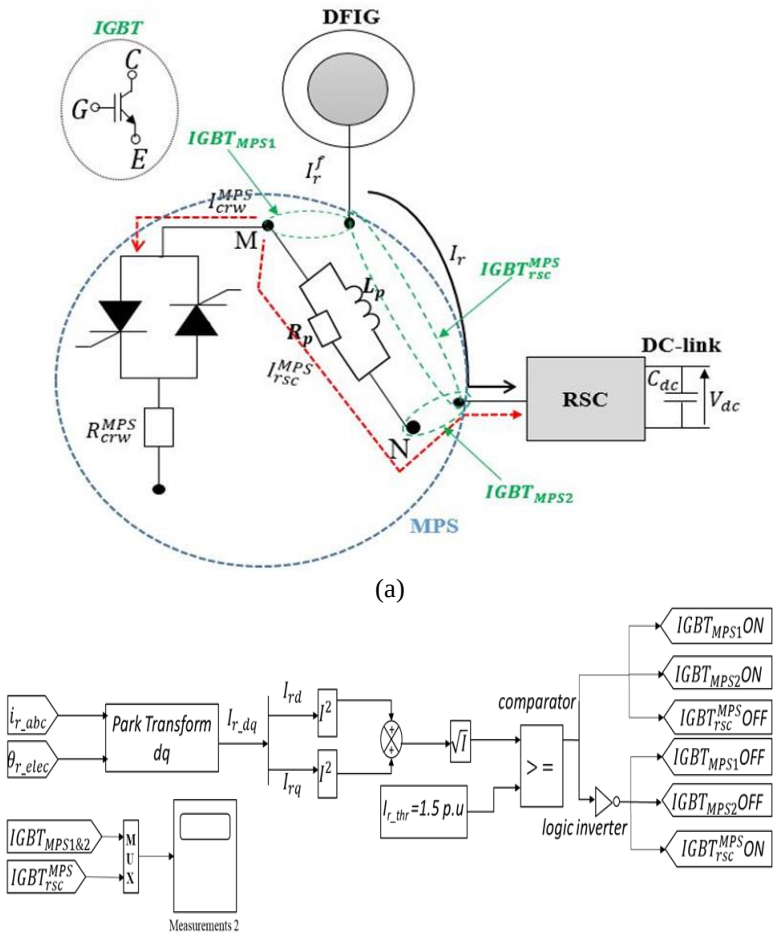

Figure. 7 Commutation architectures for: (a) MPS and (b) their IGBT's command algorithms

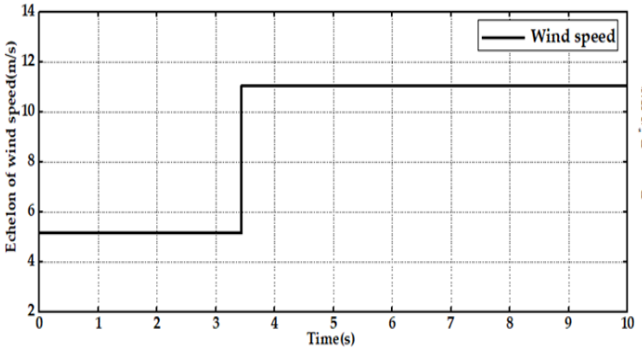

Figure. 8 Wind speed profil

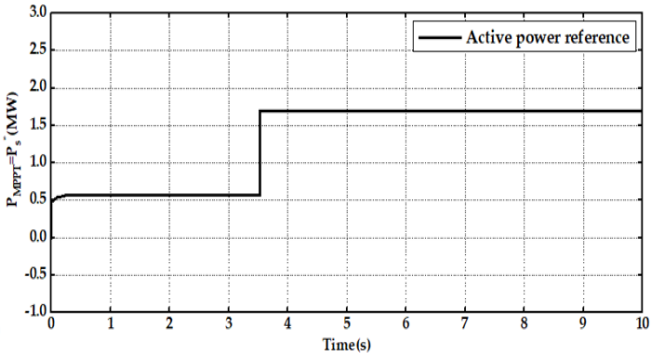

Figure. 9 Power extracted

PCC. The fault was subsequently resolved by isolating the faulty section at t = 7.62s (Fig. 10).

To demonstrate the validated responses for a 2 MW-DFIG unit, a comparative study is carried out using two scenarios: one employing the conventional crowbar protection circuit with a DC-chopper, and the other utilizing the MPS. Therefore, a comparison is performed between these two distinct responses in the absence of any protection. To ensure the activation of all protection schemes during critical failure scenarios, the rotor's limiting current is set to $I_{r\text{-}thr}$=1.5pu (maximum acceptable value). The switching command diagram of the two protection schemes is shown in Figs. 6(b) and 7(b). Through many compilations of simulation tests and the use of the test and error procedure, the optimum numbers for the parameters of R_{crw}^{c}, R_{DC_ch} and R_{crw}^{MPS}, R_p,and L_p are found and listed in Table 2 in appendix. As depicted in Fig. 11(a), the effective value **(**RMS) of stator current is approximately 5.2kA in the absence of any protection measures. However, with the implementation of the traditional crowbar and MPS

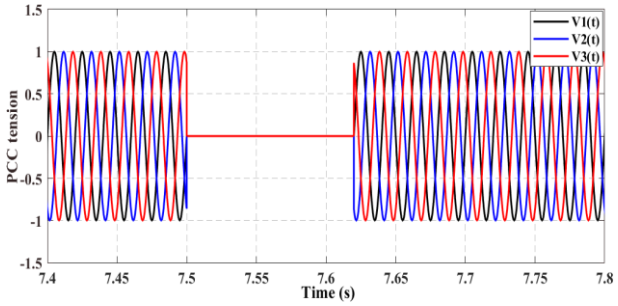

Figure. 10 Profile of PCC tension per unit (pu)

enable techniques, the RMS stator current decreases to 4.6kA and 4.8kA, respectively. Fig. 11(b), the RMS rotor current with no protection present is approximately 5.2kA while after traditional crowbar and MPS enable, it is decreased to 2.9kA and 3.1kA, accordingly. Furthermore, with MPS the RSC current reduces to below 2.9kA instead of 0.2KA with a crowbar, which demonstrates the keeping of the connection of RSC to the rotor, as seen in Fig. 11(c). In addition, when the MPS is used, its crowbar consumes 1.52kA of rotor current against 2.52kA with the standard crowbar, as illustrated in Fig.11d. It is important to emphasize that the primary purpose of employing this conventional crowbar in DFIG protection is to ensure the secure connection of the RSC to the coils of the rotor and swiftly dissipate the excessive rotor current via the earthed resistor of the crowbar. With the MPS design, the goal is to keep the RSC linked to the rotor coils. The integrated crowbar of the MPS redirects excessive current to the ground through its resistor. This mechanism absorbs a portion of the overcurrent in the rotor and assists in maintaining the RSC current within acceptable limits. Such safety tolerances exist in power electronics designs to manage transient conditions. For illustrative purposes, if the RSC threshold current were increased to twice its value (2×1.775kA), the DFIG would be able to operate no with any disconnection from the electric grid. However, the major disadvantage of the traditional crowbar is that the generator losses control during the crowbar action. By utilizing the MPS, the need to deactivate the RSC is circumvented, leading to enhanced performance in DFIG-LVRT. To ensure safety, it is crucial to keep the DC-link voltage within a safe range, specifically below 1.45pu. In Fig. 12, it is evident that the DC-link voltage reaches 1.96kV in the absence of any protection, while with the use of the MPS, the tension is reduced to a peak value of 1.4kV in comparison with the traditional protection (DC-chopper : $IGBT_{dc\_ch}$ ON) its value reduces to 0.3 kV. So the MPS can limit the V_{dc} without the use of a DC-chopper. Fig. 13 shows the dynamic response of the stator's active power under the PI controller. Initially, with crowbar protection in place, the value surges to 2MW when the fault arises, subsequently plummeting to below zero for the remainder of the fault duration. Following fault clearance, it gradually begins to rise again, displaying slight oscillations. On the other hand, with the added MPS, active power dynamics are improved especially during the fault duration, and reach 1.1 MW instead of -0.1MW with a crowbar. Fig. 14 depicts the dynamic behavior of the stator's reactive power when employing the PI controller. In the first place, with crowbar protection, the system demands a high reactive power from the grid now of fault occurrence and it decreases rapidly to a value of 5 MVAr during the rest of the fault, and then a strong oscillation after the fault occurrence. The second is that with MPS protection, the dynamic response of the stator's reactive power is improved, particularly during the fault, its value is reduced to 1.5 MVAr, then a low amplitude of oscillations is obtained after the fault is cleared, which deduces an increase in the voltage at PCC, so the wind power system remains connected to the grid. Fig. 15a and b show the different IGBT activation and deactivation pulses.

6. Conclusions

This research proposes an improved LVRT technique for wind farms using DFIG , and it is compared to the traditional crowbar protection scheme with a DC-chopper. The suggested MPS is positioned directly behind the rotor coils and the converter RSC for installation. It includes a classic crowbar and RpLp circuit in parallel. Similar to the crowbar, the MPS operates to safeguard both the RSC and the DC-link condenser, Guaranteeing the attachment of the RSC converter to the rotor and avoiding any loss of generator control. By configuring the MPS settings optimally for the RpLp parallel device with an integrated crowbar, the DFIG operates in a hybrid mode, exhibiting attributes of both a semi-SCIG and a semi-DFIG. Hence, it is essential to exercise caution when choosing the settings to meet the demands of protective features while maintaining the operation of the RSC. The comparative analysis carried out showed that the introduction of MPS can improve DFIG stability against symmetrical voltage dip. This is achieved by constraining the rotor current from 5.2 kA to 3.1 kA, thereby maintaining the DC link tension below 1.45 pu and preserving the connection between the rotor and the RSC. As a result, the DFIG's stator efficiency is also enhanced through the regulation of their powers.

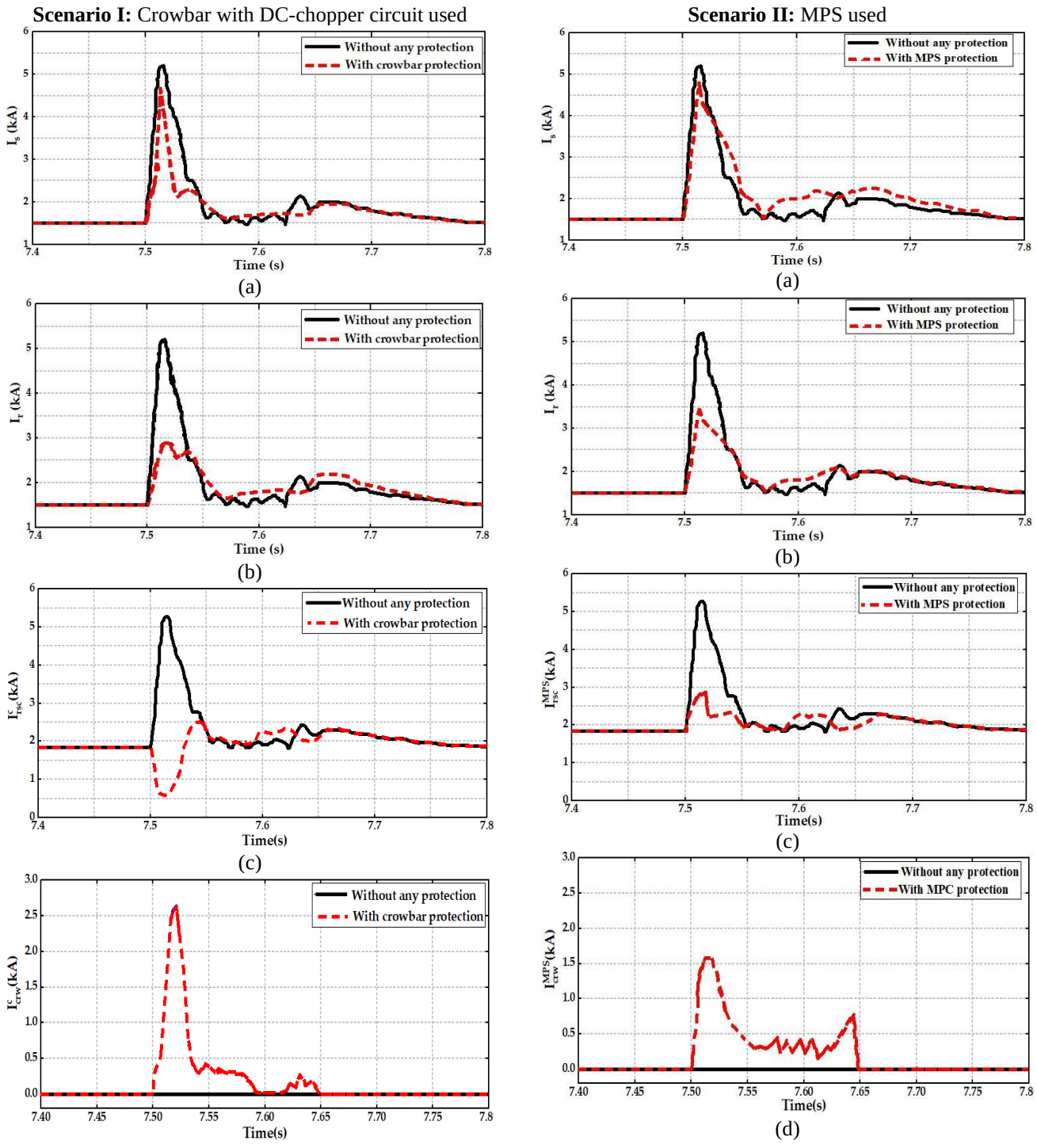

Figure. 11 Comparison of results with and no protection for the two scenarios considered; scenario I- only crowbar, and scenario II- MPS: (a) stator_current, (b) rotor_current, (c) RSC_current, and (d) crowbar_current

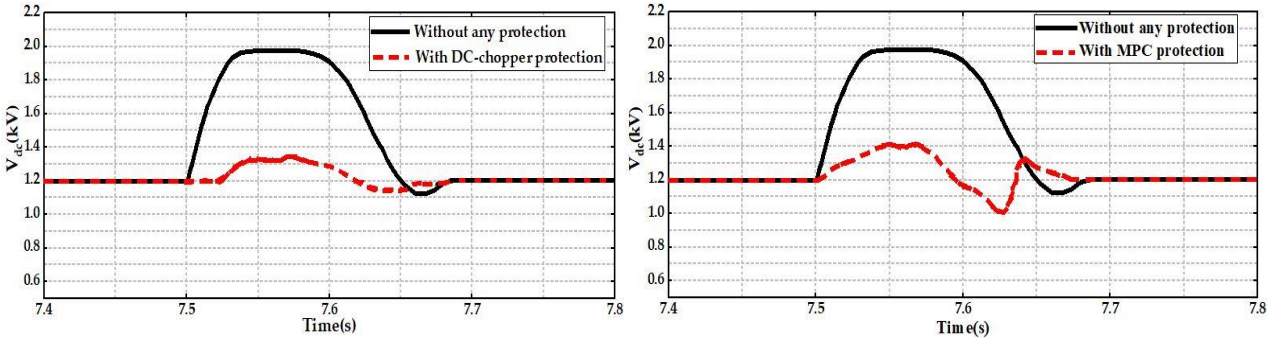

(a) (b)

Figure. 12 Comparison of results of DC-link tension with and no protection for the two scenarios considered: (a) scenario I- only DC-chopper and (b) scenario II- MPS

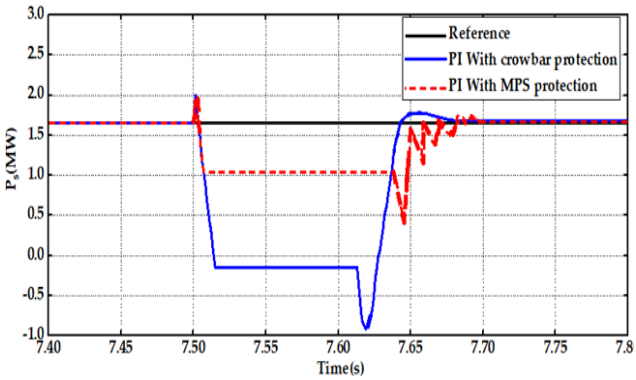

Figure. 13 Results of stator's active power comparison with PI controller for two protection schemes

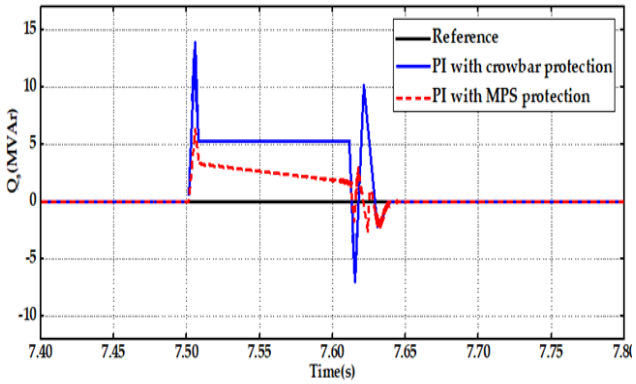

Figure. 14 Results of stator's reactive power comparison with PI controller for two protection schemes

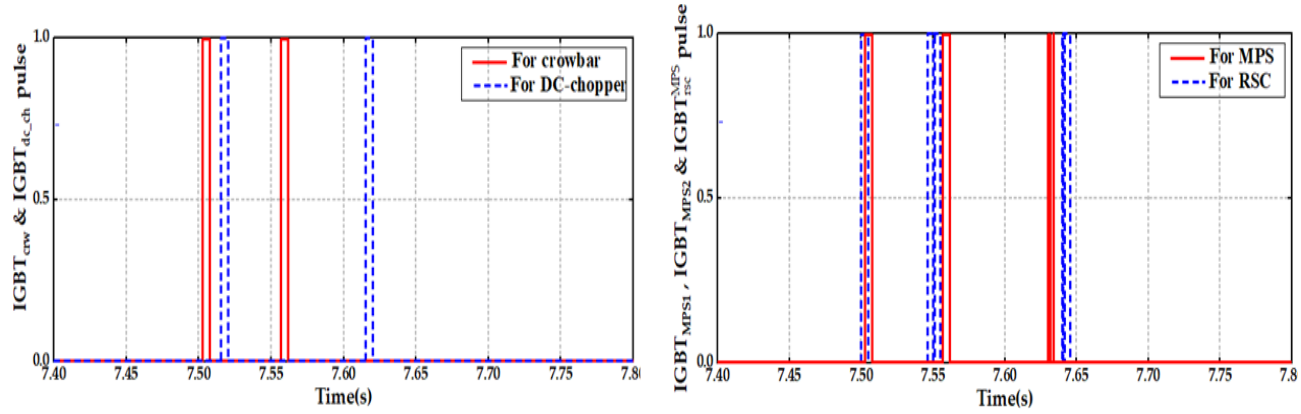

(a) (b)

Figure. 15 Command signals of: (a) $IGBT_{crw}$, $IGBT_{dc\_ch}$ and (b) $IGBT_{MPS1}$,$IGBT_{MPS2}$ and $IGBT_{rsc}^{MPS}$

Appendix

Table 2. Parameter values of crowbar classic (with DC-chopper) and MPS

Parameter	Value
R_{crw}	0.25 Ω
R_{crw}^{MPS}	0.18 Ω
R_p	10 Ω
L_p	25 H
R_{DC_ch}	0.5 Ω

Table 3. Parameter values associated with the wind turbine and DFIG

Parameter	Value
Rated power (P_n)	2 MW
Number of blades	3
Radius (R)	39m
Swept surface (S_t)	5027m^2
Air density (ρ)	1.225 kg/m^3
Gearbox (G)	90
Stator nominal voltage(V_{sn})	690 V

Nominal frequency(f)	50 Hz
Number of pole pairs(p)	2
Stator resistance(R_s)	0.023 pu
Rotor resistance(R_r)	0.016 pu
Stator inductance(L_s)	0.18 pu
Rotor inductance(L_r)	0.18 pu
Mutual inductance(M)	2.9 pu
DC-link voltage(V_{dc})	1.2 kV

Notation list

V_s ,V_r Instantaneous stator and rotor voltages
U_{pcc} Common coupling point tension
ΔV_s Variation in stator voltage during a voltage dip
ΔV_r Variation in rotor voltage during a voltage dip
I_s ,I_r Instantaneous stator and rotor currents
$I_{r\text{-}thr}$ Rotor current limit value during a voltage dip
P_s ,Q_s Active and reactive power at the stator
P_s^*, Q_s^* Stator power reference values
S Apparent power
θ_{r_elec} Rotor electrical angle
θ_{s_elec} Stator electrical angle
T_{em}^* Reference electromagnetic torque
C_{dc} DC-link capacitance
R_f ,L_f Resistance and inductance of the filter
ω_s ,ω_{slip} Stator angular frequency, slip angular frequency
Ω_m Mechanical speed
p Number of pole pairs
v_w Wind speed
R_p ,L_p Resistance and inductance of parallel impedance
V_{sd} ,V_{sq} Stator voltage in the direct and quadrature axes
V_{rd} ,V_{rq} Rotor voltage in the direct and quadrature axes
I_{rd} ,I_{rq} Rotor current in the direct and quadrature axes
I_{sd} ,I_{sq} Stator current in the direct and quadrature axes
R_{crw} Resistance of conventional crowbar
R_{crw}^{MPS} Resistance of MPS crowbar
k_p ,k_i Controller constants

Abbreviation

WT : Wind turbine
WF : Wind farm
DFIG : Doubly fed induction generator
SCIG : Squirrel Cage Induction Generator
RSC : Rotor-side converter
GSC : Grid-side converter
AC : Alternating Current
DC : Direct current
dq : Direct-quadrature
PCC : Point of common coupling
MPPT : Maximum power point tracking
PWM : Pulse width modulation
PLL : Phase -locked loops
MUX : Multiplexer
LVRT : Low voltage ride-through
FRT : Fault ride through
PI : Proportional-integral
Th : Thyristor
D : Diode
MPS : Modified protection scheme
IGBT : Insulated-gate bipolar transistor

Conflicts of interest

The authors declare no conflict of interest.

Author contributions

All authors have evenly participated in conceptualizing the study, developing the methodology, validating the findings, acquiring resources, preparing the original draft, reviewing and editing it for this research work.

References

[1] M. Mossa, *Modeling Analysis and Enhancement of the performance of a Wind Driven DFIG During steady state and transient conditions*, Anchor Academic Publishing, German, 2014.

[2] E. Chetouani, Y. Errami, A. Obbadi, and S. Sahnoun, "Design of Optimal Backstepping Control for a Wind Power Plant System Using the Adaptive Weighted Particle Swarm Optimization", *International Journal of Intelligent Engineering and Systems*, Vol. 14, No. 6, pp. 125–136, 2021, doi:10.22266 /ijies2021.1231.12.

[3] N. H. Saad, A. A. Sattar, and A. M. Mansour, "Low voltage ride through of doubly-fed induction generator connected to the grid using sliding mode control strategy", *Renew. Energy*, Vol. 80, pp. 583–594, 2015, doi: 10.1016/j.renene.2015.02.054.

[4] S. Li, T. A. Haskew, K. A. Williams, and R. P. Swatloski, "Control of DFIG wind turbine with direct-current vector control configuration", *IEEE Transactions on Sustainable Energy*, Vol. 3, No. 1, pp. 1–11, 2012, doi: 10.1109 /

TSTE.2011.2167001.

[5] B. Rached, M. Elharoussi, and E. Abdelmounim, "Fuzzy logic control for wind energy conversion system based on DFIG", In: *Proc. of International Conf. on Wireless Technologies, Embedded and Intelligent Systems*, Fez, Vol. 2, No. 1, pp. 1–6, 2019, doi: 10.1109/WITS.2019.8723722.

[6] A. Touati, E. Abdelmounim, M. Aboulfatah, A. Moutabir, and R. Majdoul, "Improved strategy of an MPPT based on the torque estimator for variable speed turbines", *International Review on Modelling and Simulations*, Vol. 8, No. 6, pp. 620–631, 2015, doi: 10.158 66/iremos.v8i6 .7122.

[7] O. S. Adekanle, M. Guisser, E. Abdelmounim, and M. Aboulfatah, "Observer-Based Adaptive Backstepping Control of Grid-Connected Wind Turbine Under Deep Grid Voltage Dip", *Recent Advances in Electrical and Information Technologies for Sustainable Development, Advances in Science, Technology & Innovation*, No. 2, pp. 75–84, 2019, doi: 10.1007/978-3-030-05276-8_9.

[8] B. Qin, H. Li, X. Zhou, J. Li, and W. Liu, "Low-voltage ride-through techniques in DFIG-based wind turbines: A review", *Applied Sciences*, Vol. 10, No. 6, 2020, doi: 10.3390 /app 10062154.

[9] S. Yamparala, L. Lakshminarasimman, and G. S. Rao, "Improvement of LVRT Capability for DFIG based WECS by Optimal Design of FoPID Controller using SLnO + GWO Algorithm", *International Journal of Intelligent Engineering and Systems*, Vol. 16, No. 1, pp. 202–213, 2023, doi: 10.22266 /ijies 2023.0228.18.

[10] A. Loulijat, N. Ababssi, and M. Makhad, "Kalman Observer Contribution to a Second Order Sliding Mode Control for Wind Turbine Based on DFIG During the Network Voltage Dip", *International Journal of Intelligent Engineering and Systems*, Vol. 14, No. 5, pp. 88–101, 2021, doi:10.22266 /ijies 2021.1031.09.

[11] O. Noureldeen, "Behavior of DFIG Wind Turbines with Crowbar Protection under Short Circuit", *International Journal of Electrical & Computer Sciences IJECS-IJENS*, Vol. 12, No. 03, pp. 129103–6868, 2012.

[12] G. Pannell, D. Atkinson, B. Zahawi, and S. Member, "Minimum-Threshold Crowbar for a DFIG Wind Turbine", *IEEE Transa Ctions on Energy Conversion*, Vol. 25, No. 3, pp. 750–759, 2010.

[13] M. J. Harandi, S. G. Liasi, E. Nikravesh, and M. T. Bina, "An Improved Control Strategy for DFIG Low Voltage Ride-Through Using Optimal Demagnetizing method", *2019 10th Int. Power Electron. Drive Syst. Technol. Conf. PEDSTC 2019*, pp. 464–469, 2019, doi: 10.1109/PEDSTC.2019.8697267.

[14] J. Yang, J. Fletcher, and J. O. Reilly, "A series-dynamic-resistor-based converter protection scheme for doubly-fed induction generator during various fault conditions", *IEEE Transactions on Energy Conversion*, Vol. 25, No. 2, pp. 422–432, 2010, doi: 10.1109/TEC .2009.2037970.

[15] A. Loulijat, N. Ababssi, and M. Makhad, "DFIG use with combined strategy in case of failure of wind farm", *International Journal of Electrical and Computer Engineering*, Vol. 10, No. 3, pp. 2221–2234, 2019, doi: 10.11591/ijece.v10i3.pp2221-2234.

[16] O. S. Adekanle, M. Guisser, E. Abdelmounim, and M. Aboulfatah, "Nonlinear Controller with Rotor Crowbar and DC-Chopper Fault Ride Through Technique for Grid-Connected Doubly-Fed Induction Generator", *International Review of Automatic Control* ,Vol. 11, No. November, pp. 281–292, 2018.

[17] K. Okedu, S. Muyeen, R. Takahashi, and J. Tamura, "Wind farms fault ride through using DFIG with new protection scheme", *IEEE Transactions on Sustainable Energy*, Vol. 3, No. 2, pp. 242–254, 2012, doi:10.1109/TSTE .2011.2175756.

[18] Z. C. Zou, X. Y. Xiao, Y. F. Liu, Y. Zhang, and Y. H. Wang, "Integrated Protection of DFIG-Based Wind Turbine with a Resistive-Type SFCL under Symmetrical and Asymmetrical Faults", *IEEE Transactions on Applied Superconductivity*, Vol. 26, No. 7, pp. 1–5, 2016, doi: 10.1109 /TASC. 2016. 25 74352.

[19] O. Adekanle, M. Guisser, E. Abdelmounim, and M. Aboulfatah, "Adaptive backstepping control of grid-connected doubly-fed induction generator during grid voltage dip", In: *Proc. of International Conf. on Electrical and Information Technologies*, pp. 1–6, 2018, doi: 10.1109/EITech.2017.8255267.

[20] Y. Wang, Q. Wu, H. Xu, Q. Guo, and H. Sun, "Fast coordinated control of dfig wind turbine generators for low and high voltage ride-through", *Energies*, Vol. 7, No. 7,pp. 4140–4156, 2014, doi: 10.3390 /en7074140.

[21] D. V. N. Ananth and G. V. N. Kumar, "Fault ride-through enhancement using an enhanced field oriented control technique for converters of grid connected DFIG and STATCOM for different types of faults", *ISA Transactions*, Vol.

62, pp. 2–18, 2016, doi: 10.1016/j.isatra.2015.02.014.

[22] S. S. A. Alhalim and L. A. Alnabi, "Enhancement transient stability of wind power system of doubly-fed induction generator using STATCOM and PI controller", *International Journal of Power Electronics and Drive Systems*, Vol. 10, No. 4, pp. 1977–1985, 2019, doi: 10.11591 /ijpeds .v10.i4.pp1977-1985.

[23] A. R. A. Jerin, P. Kaliannan, and U. Subramaniam, "Improved fault ride through capability of DFIG based wind turbines using synchronous reference frame control based dynamic voltage restorer", *ISA Transactions*, Vol. 70, pp. 465–474, 2017, doi: 10.1016 /j. isatra.2017.06.029.

[24] A. Touati, E. Abdelmounim, M. Aboulfatah, A. Moutabir, and R. Majdoul, "Improved strategy of an MPPT based on the torque estimator for variable speed turbines", *International Review on Modelling and Simulations*, Vol. 8, No. 6, pp. 620–631, 2015, doi: 10.158 66/iremos.v8i6 .7122.

[25] A. Loulijat, H. Chojaa, M. E. Marghichi, N. Ettalabi, A. Hilali, A. Mouradi, A. Y. Abdelaziz, Z. M. S. Elbarbary, and M. A. Mossa, "Enhancement of LVRT Ability of DFIG Wind Turbine by an Improved Protection Scheme with a Modified Advanced Nonlinear Control Loop", *Processes*, Vol. 11, p. 1417, 2023, https://doi.org /10.3 390 /pr 1105 1417.